

**Test of Four Coil Helical Solenoid Magnet HSM01 TD-09-011**

M. Tartaglia, G. Chlachidze, V.S. Kashikhin, F. Lewis, M. J. Lamm, A. Makarov,  
I. Novitski, D. Orris, C. Sylvester, J. C. Tompkins, D. Walbridge, M. Yu

**Outline**

1. Introduction
2. Fabrication Overview
3. Test Overview
4. Magnetic Measurements
5. Quench Studies
6. Heater Protection Study
7. RRR
8. Strain Gauge Measurements
9. Post-Test Inspections and Autopsy
10. Conclusions
11. References

**1. Introduction**

HSM01 is a prototype four-coil superconducting helical solenoid magnet. It was built to test design concepts and explore manufacturing and performance issues, as the first step in developing a long and large aperture helical solenoid magnet for a muon cooling channel [1]-[2]. Details of the four-coil solenoid magnetic and mechanical design are discussed in [3].

There were several important goals for this magnet test: 1) to map the magnetic field in 3 dimensions, and compare it to model predictions; 2) measure cool-down and excitation strain and stress changes on the coils and structure, for comparison with mechanical models; 3) test the quench performance of the coils, which were wound and epoxy-impregnated but not subjected to pre-load force constraints; 4) study quench temperature dependence to determine whether performance is mechanical or conductor limited; 5) study ramp rate dependence of quench current to find whether eddy current effects are important in this non-laminated structure; 6) study the effectiveness of strip heaters to induce quenches for magnet protection; 7) determine RRR of the conductor (which affects stability and quench development properties).

**2. Fabrication Overview**

The helical solenoid design parameters are given in Table 1. A cross sectional view of the magnet with as-built dimensions is shown in Figure 2.1. Three of the coils were wound with 9 turns of SSC-inner cable; the fourth (coil 3) was (believed to have been, based upon resistance measurements, but not confirmed by coil inductances) wound with one extra turn. Coils are sequentially numbered 1 through 4, with coil 1 at the Lead End (LE) and coil 4 at the non-lead end. Electrical, mechanical, and magnetic details and a test overview were captured in the Magnet Description Document in preparation for testing the magnet in the Test & Instrumentation Department Vertical Magnet Test Facility (VMTF), which is available on the T&I web site at

<http://tiweb.fnal.gov/website/controller/404>.

**Table 1: Solenoid Parameters**

Parameter	Units	Value
Coil inner diameter	mm	426
Coil outer diameter	mm	455
NbTi superconducting cable	mm	12.34 x 1.46
Cable critical current at 7 T, 4.2 K	A	9660
J <sub>c</sub> (non-Cu)	A/mm <sup>2</sup>	1730
Copper to superconductor ratio		1.5:1
Strand diameter	mm	0.8
Helical orbit radius	mm	255
Number of turns per coil		10
Coil width	mm	20

A number of issues arose during fabrication which affected the test program. First, there were difficulties with electrical insulation of the coils from ground. It is typical for insulation to withstand a 1000 V to ground hi-pot test in air at room temperature, with leakage current less than 1  $\mu$ A. Prior to vacuum impregnation of the assembled coil structure, the magnet passed hi-pot with no leakage current; after impregnation however, this magnet failed hi-pot above 250 V. Following the final outer skin welding step, hi-pot performance degraded even further: It was improved (briefly) to 500 V by manipulating and potting the negative Sc Lead (which is connected to coil 1). After mounting the magnet to the VMTF 15kA Top Plate Assembly, which required further manipulation of the Sc Leads, the leakage current to ground was measured to be at least 18  $\mu$ A at 250 V. After the cool down to 4.5 K, the problem degraded to a 15 k $\Omega$  short to ground. Further discussion of this problem is provided in Section 3.

The protection heaters consisted of 1/2-inch wide x 5-mil thick copper-clad stainless steel strips encapsulated in 1-mil thick Kapton® insulation; they were installed in the gap outside the outer coil radius after the coils were wound, but before epoxy impregnation (thus, good contact with the coils was *not* assured). Three heaters extended around nearly the entire coil outer perimeter, while one heater was only 6 inches long (therefore it was more of a “spot” heater). Two issues required some special treatment in the cold test: First, because of the coil-to-ground hi-pot issue, there was concern about generating voltage in the coil by inducing a quench. Second, the “spot” heater for coil 4 had only half the resistance of the other heaters. Consequently, all of the individual leads for powering heaters were wired to the instrumentation tree, in order to give the greatest flexibility in defining the circuits for the heater test program.

Figure 2.2 shows the solenoid under construction, with the positive and negative superconducting leads emerging from the coils; the positive lead (connected to coil 1) emerges straight out, while the negative lead ramps up from the final winding. This figure indicates the direction of the coil windings within the solenoid, which defines the field direction. It also shows the offsets of the individual coils (with respect to the leads, and other physically identifiable features on the structure).

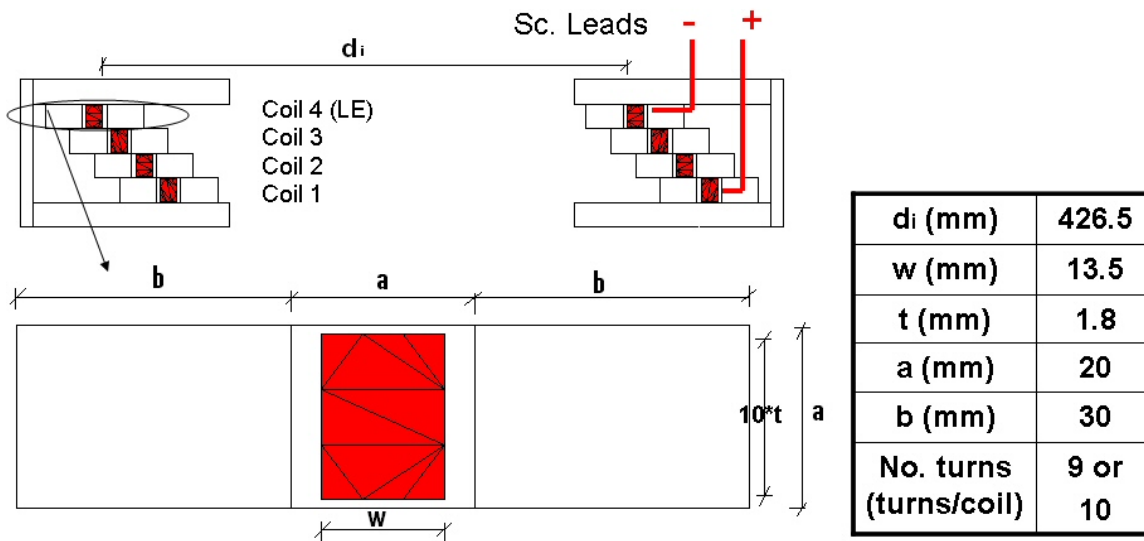


Fig. 2.1. HSM01 structure, coil cross sections, and dimensions



Fig. 2.2. HSM01 coils during solenoid fabrication.

### 3. Test Overview

The magnet was delivered to IB1 for instrumentation wiring and warm magnetic measurements on September 22. Warm magnetic measurements were performed on test stand B in the Magnet Test Facility (MTF), and were finally completed on November 6 after much effort to align and survey the magnet and probe, and solve Hall probe 3D motion and readout problems. After an inspection of the coil positions was made in IB4, in IB2 the outer skin was welded on, and the solenoid was returned to IB1 November 11 for cold testing.

The cold test of HSM01 was performed in the VMTF using the “15kA” top plate assembly (with Lambda plate) and “HGQ” warm bore installed; the magnet was oriented with the LE facing up. Warm electrical checkout was completed on 11/17, and the magnet was cooled down directly to 4.5K (no LN2 pre-cooling) on 11/19. Once cold, the coil-to-ground hi-pot attempt failed at only 10 V (1 $\mu$ A criteria); subsequently attempts were made to try to localize the short to ground by warming above the transition temperature and making 4-wire voltage to ground measurements. However, when warmed to 12 K, the short disappeared. The magnet was cooled to 4.5 K again on November 24, but power supply regulation problems prevented ramping to quench. Finally on 11/25 it was possible to ramp and complete the cold checkout of the quench protection system. Shortage of liquid helium (due to competition from VTS RF cavity test activities) and the Thanksgiving holiday caused further delays, so quench training at 4.5 K began on 12/1 and continued on 12/2.

When cool down to 3 K was attempted on 12/3, contamination levels from a leak at the Kinney Pump 1 caused the need for a 100 K warmup of the cryogenic plant cold box. (Dirty gas was stored in Buffer Tank #1, which allowed the plant to start up and continue operating, but this in fact limited the ability of operators to fully control temperatures at VMTF). The plant recovery was successful and liquid helium inventory was built up on Friday 12/5. Special efforts were made to complete the cold test program on Saturday 12/6: the magnet was cooled to 3.0 K for studies of quench temperature dependence. It was not possible for operators to warm up to 4.5 K quickly (which required gas from the Buffer Tank#1, which was contaminated); so, some heat was added by training quenches to raise the temperature to 4.0 K, where ramp rate dependence and basic heater effectiveness tests were made.

The magnet was kept cold until Monday 12/8, in order to set up and capture RRR data. The warm up began mid-morning on 12/8, and reached room temperature over the weekend, 12/13. Room Temperature RRR data were captured Monday 12/15 and the assembly was removed from the VMTF Dewar. Inspection of the top plate assembly and magnet showed a large amount of debris around the power leads, from shattered glass tape, RTV, and insulation material; it was evident that the Sc Lead (glass tape) restraints had broken, and the negative Sc Lead had arced to ground through contact with a nut on one support rod. The reason for this was clearly inadequate Sc Lead support to resist the Lorentz forces in the very large fringe field of the magnet at high current (an uncommon situation, having no iron yoke to contain the field). A detailed study of this was made, and an incident report has been written and posted on 12/24 to the Test & Instrumentation department web page at

<http://tiweb.fnal.gov/website/controller/468>.

Following the holiday period, on 1/5/09, the magnet was sent back to IB4 to re-measure the coil positions (needed to relate them to the Hall probe measurement coordinate system). This turned out to be difficult – interference from flanges prevented making measurements of one coil; thus, its center position was interpolated from the other ring measurements. These center positions were used for modeling the magnetic field for comparison to data (section 4f).

#### 4. Magnetic Measurements

##### a. Overview

Figure 4.1 shows the Helical Solenoid mounted on test stand B in MTF, with the coordinate system for magnetic measurements shown. The X and Y axes were defined by tooling balls and scribe lines on the Lead End (LE) surface; since the coils are offset rings, there is no “center” or axis of symmetry, so  $X=Y=0$  is somewhat arbitrarily chosen in the aperture middle. The same LE top surface also defines the reference plane for  $Z=0$ , and the right-handed coordinate system puts the body of the magnet (and peak field) at negative Z. It should be noted that this coordinate system was added late in the fabrication – it had not been planned for earlier in the design – and therefore the circular coil center positions were not known in advance of the measurements; also, it was not recognized what difficulties would be encountered in setting up to perform the measurements, or in relating the coordinates later to the magnetic model. Trying to finally get this right required scrutiny of fabrication photographs, study of drawings of the 3D probe, correction of drawings made from inspection measurements, and adjustments of model geometry. Thus, if magnetic measurements are important in future helical magnets, it is necessary to focus on these details early in the process.

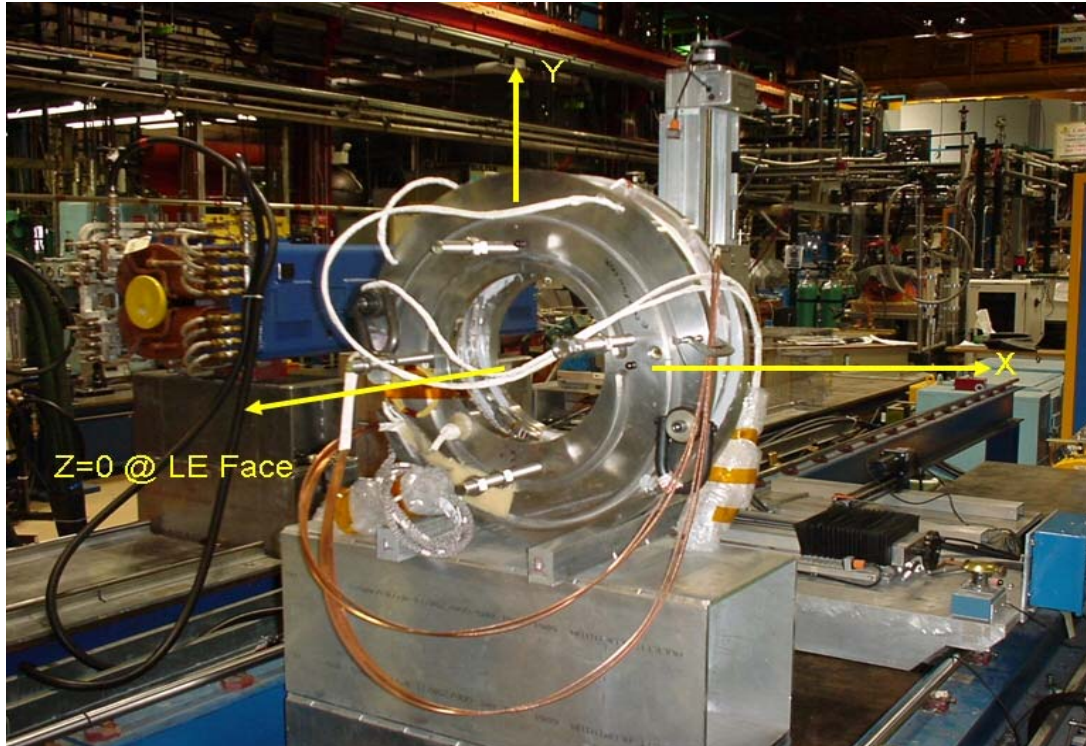


Fig. 4.1. HSM01 mounted upright on test stand B for 3-axis warm Hall probe warm measurements, and illustrating the coordinate system.

### **b. Warm Magnetic Measurements**

Test Stand B is equipped to provide motion in three dimensions and readout of a 3-axis Hall probe array. This provided the only means for carefully mapping the field in a volume extending out to large radii (near the coils) and large distance (~0.5 meter) from the coil center. The Hall probe array contains 3 1-dimensional Group3 Hall probes which are mounted in a holder that positions them in orthogonal orientations, so the active elements are not precisely at the same point and the size of the holder (and its support arm) limits the transverse motion inside the solenoid body (due to interferences with the structure at large radius). The probe position offsets are relatively small: The X spot is highest. It is 38 mils, or about 1 mm, above the Z spot. The Z spot is 107 mils, or about 2.7 mm, above the Y spot, which is on the bottom. Looking from the side, the X spot is directly over the Y spot, and the Z spot is 107 mils, or about 2.7 mm, in front of the X and Y spots. The magnet was oriented and aligned with survey to guarantee that the probe motions were, in fact, in the magnet coordinate system. The reported probe X,Y,Z positions correspond to those of the Z Hall probe.

The range of motion in a given Z scan is limited to 11 inches; therefore three sets of scans were performed with offsets in the initial Z position to cover the full range. At each Z position in a scan, the probe was positioned and field strengths recorded along the central axis ( $X=Y=0$ ), and at a radius of 4 inches every 45 degrees starting from the X axis. Each set of measurements was recorded twice, once at +10 A and once at -10 A current in the solenoid, to eliminate background fields by averaging the two polarities. The Z motion did not go precisely as programmed: first, a loose screw caused a slight backlash in the motion, so that the first few points in each segment did not move as far as they should have. Second, the last scan at positive Z was inadvertently positioned with a smaller offset than desired; this resulted in a 2 inch overlap with the previous scan (giving redundant measurements), and that the maximum positive Z reached was 2 inches less than planned (not a big deal).

Further complicating the warm measurement data, and comparison with cold measurements and magnetic model predictions, the warm 3D Hall probe coordinate system differs from the “magnet” and “motion” coordinate system defined in Figure 4.1 above. The probe has a right-handed coordinate system where  $X_{\text{probe}} = -X_{\text{motion}}$ ,  $Y_{\text{probe}} = Y_{\text{motion}}$ , and  $Z_{\text{probe}} = -Z_{\text{motion}}$ .

### **c. Cold Magnetic Measurements**

The 3-axis Hall probe used for cold magnetic measurements was a 10 T range Senis/GMW probe, serial number 26-05 (also known as the “old probe”, since a newer version is also in the MTF probe inventory), which consists of three independent Hall probes within a 0.1 mm-scale integrated circuit that is dimensionally referenced within the mechanically package. The probe thus measures the 3D field simultaneously at the same location. The probe voltages were digitized using a Keithley 2700 multiplexing DMM, which was read out and saved using a Labview program on a Windows PC. The nominal probe sensitivity, consistent with past calibrations, is 1 V/T; offsets for each channel are obtained by making measurements with no current in the magnet.

It is hard to know the precise transverse probe position with respect to the magnet coordinate system. Figure 4.2 shows the solenoid suspended on the VMTF top plate assembly with the insulated warm bore tube passing through the magnet aperture. The

warm bore position is constrained by a conical seal located at the Lambda plate (and its own stiffness). The probe was mounted in a holder that oriented it at the end of a long shaft, which had an attached scale for measuring the local Z position from the top; there is the possibility of a slight tilt of the probe in the holder, which may result in a transverse field component if the probe is not perfectly perpendicular to the main field component  $B_z$ . The shaft was centered with bearings inside the warm bore *inner* tube; a visual inspection of the warm bore *outer* tube was made and it appears to have been centered with respect to the X and Y scribe lines to within  $\sim 1$  mm. The X and Y directions were transferred from the magnet to the top plate (as well as could be done, but with unknown accuracy) and the probe was oriented via marks on the long shaft that corresponded to the probe Y axis (again, with unknown accuracy). These marks were visually kept aligned with the top plate marks during measurements. The probe orientation was such that magnet and probe X coordinates were aligned, while Y and Z coordinates were aligned with  $-Y$  and  $-Z$  of the magnet system (data have been corrected for this).

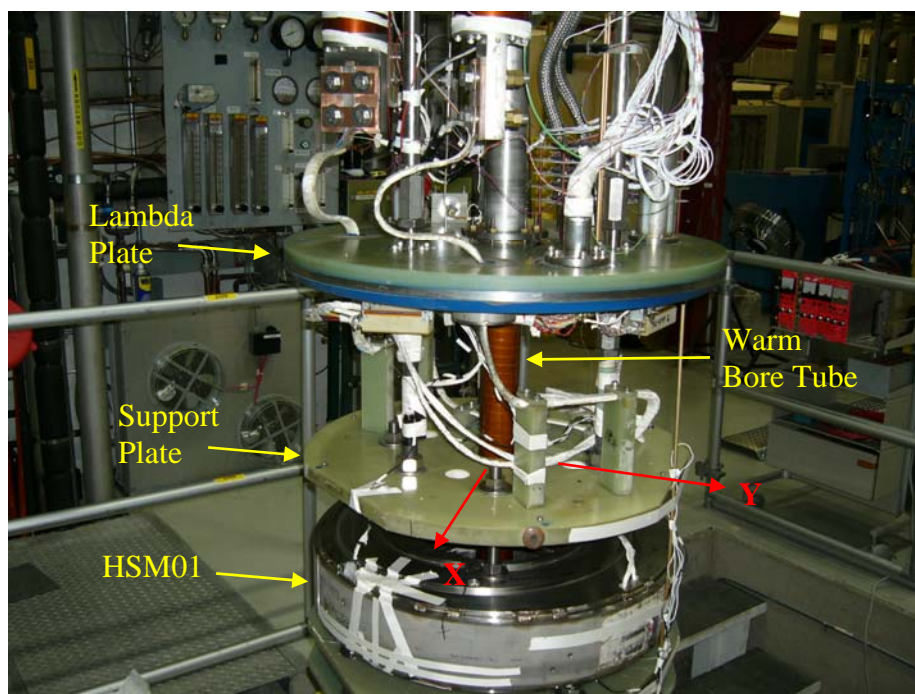


Fig. 4.2. HSM01 suspended from the VMTF top plate assembly prior to cold testing.

Figure 4.3 illustrates the coordinate systems for the magnet, motion, warm and cold Hall probes, to help clarify the relationship between the various elements. Note that the axial field direction,  $B_z$ , is directed towards  $-Z$  when the magnet is excited by a positive current (Positive lead connected to Positive PS terminal). In order to compare measurements to the magnetic model predictions (described in the next section), we need to choose a consistent polarity for the current. Since the magnetic model predicts  $B_z$  as positive, we present data for the case of negative current (thus, labels are  $-B_z$ ,  $-B_x$ ,  $-B_y$ ).

3D Warm Probe  
Measurement FRAME

3D Cold Probe  
Measurement FRAME

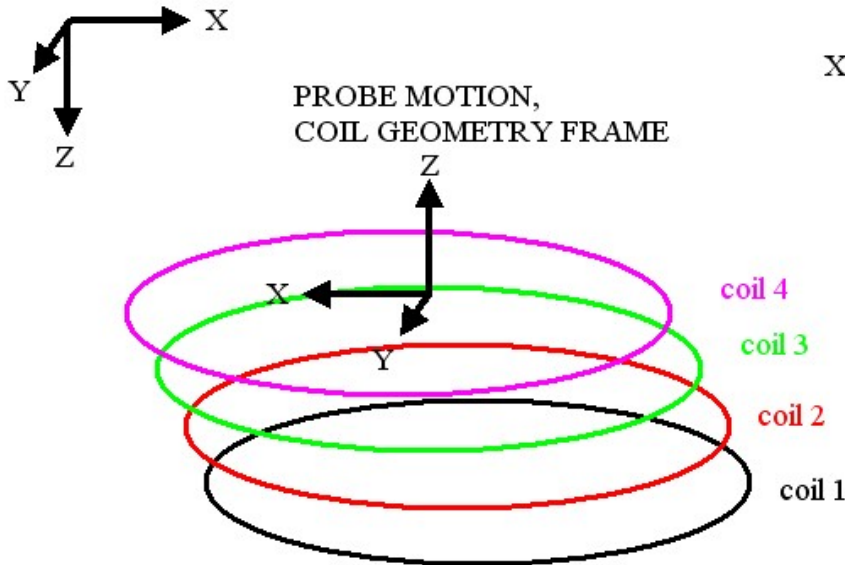


Fig. 4.3. HSM01 Coil Geometry, Probe motion, and Hall probe coordinate systems.

**d. Peak Transfer Function and Fringe Field at VMTF surface**

Figure 4.4 shows the axial and transverse field transfer functions as a function of current when the probe was positioned at the location of the peak axial field. Measurements were taken early in the cold test, first at 0 A and then on plateaus every 500 A up to 2000 A. Higher currents were not explored due to hi-pot and ground current concerns, and due to the expectation of linear behavior with current (lacking an iron flux return). The field offset levels for all three directions were all about -0.3 mV (they have been subtracted from these plots), and the noise levels are about 1 mV corresponding to ~10 G. The peak axial field is linear with current, and the transfer function is 1.060 G/A.

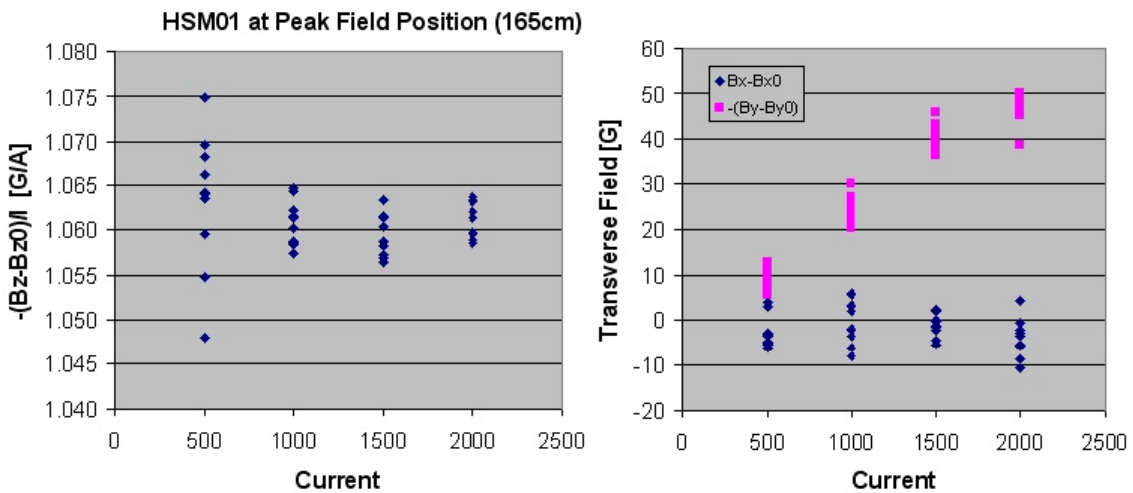


Fig. 4.4. Cold axial field transfer function (left) and transverse field strength (right) versus current at the peak field position.

**e. Measured Solenoid Field Profiles**

The Z position of cold measurements is shifted by a constant offset to match the peak axial field position from warm magnetic measurements. The resulting overlay is shown in Figure 4.5, for cold profile scan at 2000 A compared to the average of warm scans at  $\pm 10$  A, for data taken along the Z axis. The warm off-axis axial transfer function measurements are shown in Figure 4.6.

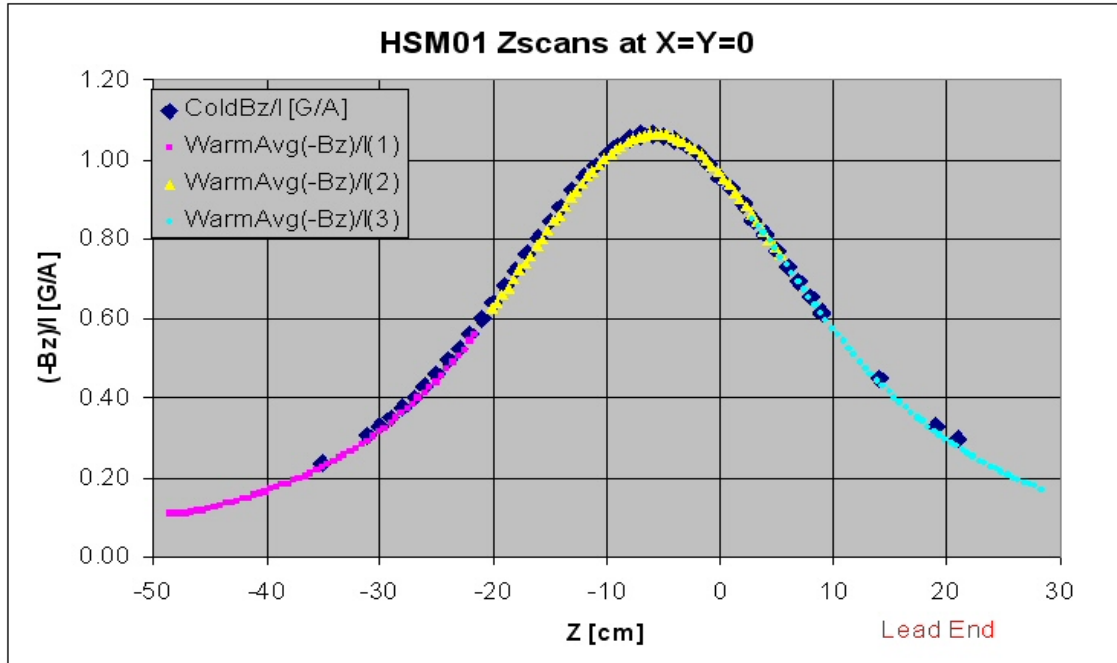


Fig. 4.5. Bz vs Z on the X=Y=0 central axis. Note that for positive current, the axial field is directed towards negative Z (hence the axis is labeled as -Bz/I).

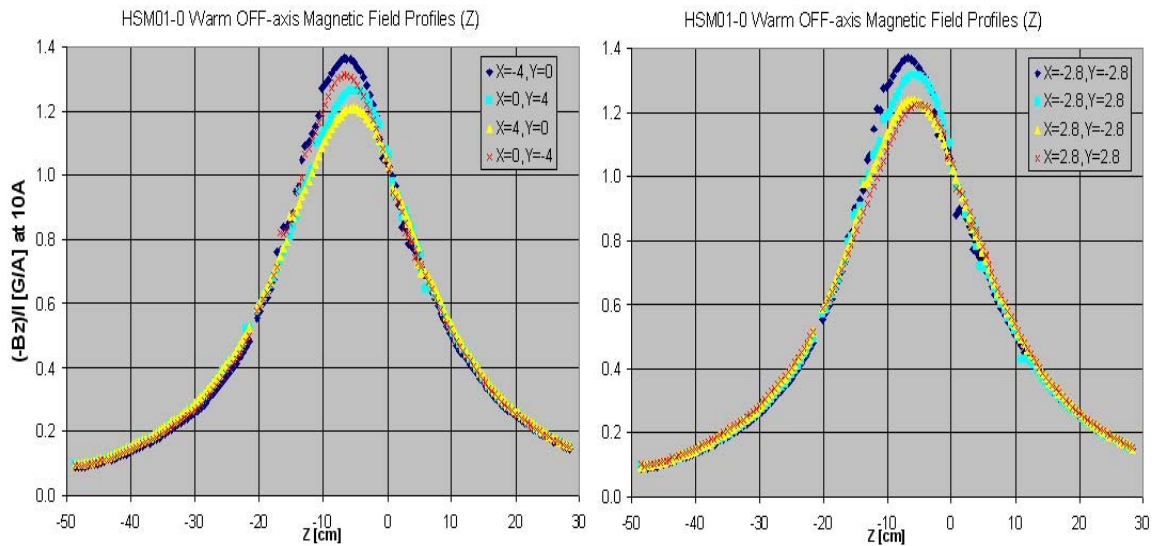


Figure 4.6. Axial field transfer function  $(-Bz)/I$  vs Z at radius of 4 inches, along the X and Y axes (left) and along 45° diagonals (right).

The transverse field measurements are shown in Figures 4.7 (warm and cold overlay for data on the Z axis), 4.8 (warm  $B_x$  data at 4 inch radius), and 4.9 (warm  $B_y$  data at 4 inch radius). While the warm and cold  $B_y$  terms agree pretty well, there is some slight but apparent disagreement between the warm and cold  $B_x$  profiles; this might be the result of cold measurement probe having a slight tilt (hence measuring a small fraction of the axial field), or being slightly off-center in the X direction.

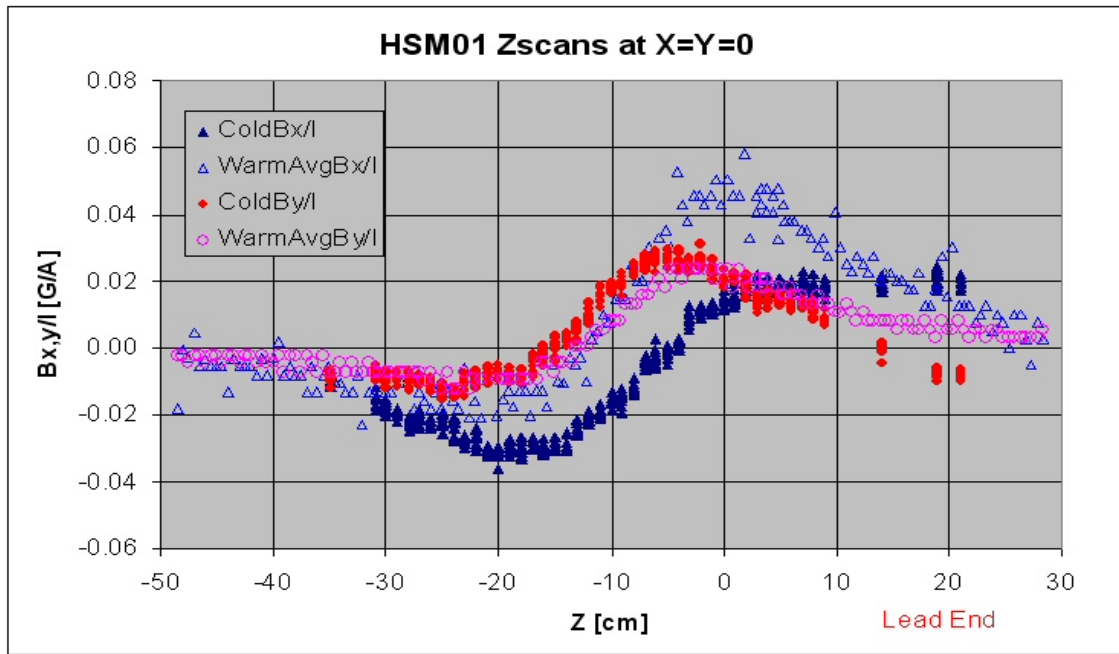


Figure 4.7. Warm and Cold  $B_x/I$  and  $B_y/I$  vs  $Z$  on  $X=Y=0$  axis.

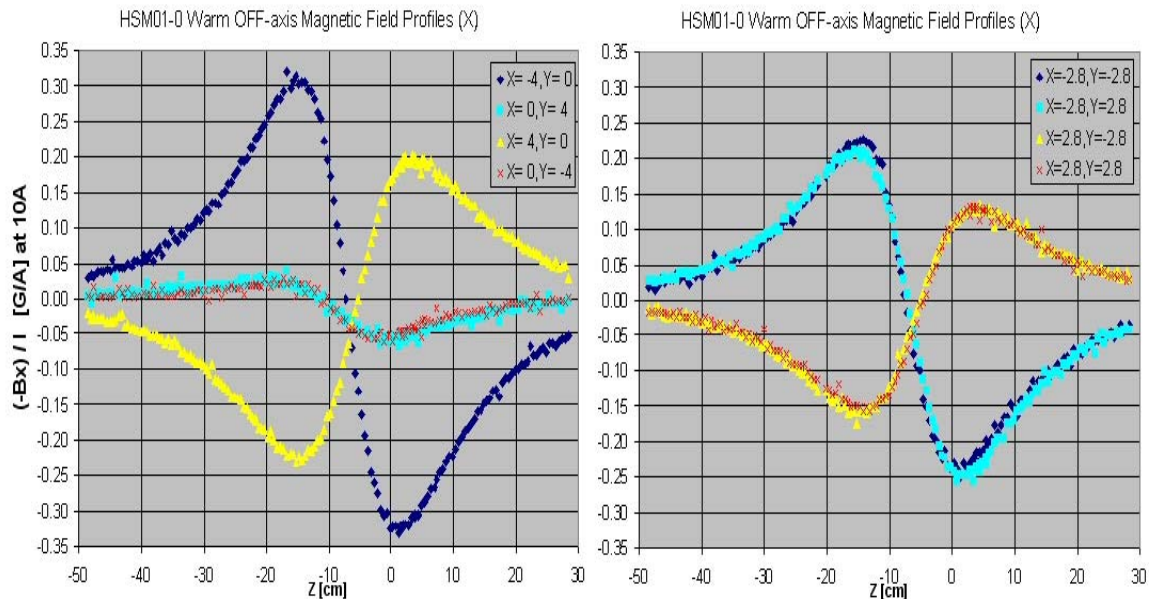


Figure 4.8. Warm transfer function  $(-B_x)/I$  vs  $Z$  at 4 inch radius on  $X$  and  $Y$  axes (left) and along  $45^\circ$  diagonals (right).

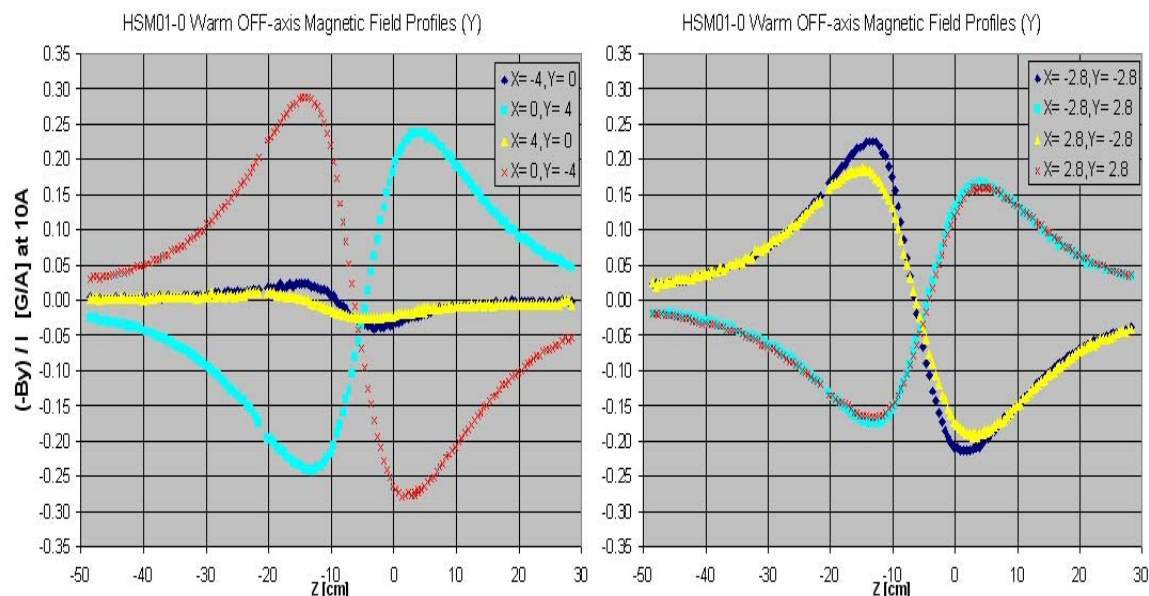


Figure 4.9. Warm transfer function  $(-B_y)/I$  vs  $Z$  at 4 inch radius on X and Y axes (left) and along 45° diagonals (right).

### f. Magnetic Data to Model Comparison

Coordinates were measured on the coil support rings following the test completion at VMTF, in order to estimate the coil center positions for the magnetic model. This was difficult, due to interference of the outer flanges, so only three of the four could be measured and the center of coil 3 was interpolated. After the test, the solenoid was cut apart for autopsy (see Section 9), and it was determined unambiguously that coil 2 had 10 turns, while all others had 9 turns of superconductor cable.

Given this information, a magnetic model was constructed in TOSCA, and predictions were made for the field shapes along Hall probe trajectories measured in MTF. The model predicts shapes and strengths that are very similar to the measured ones, but there are clearly problems with field (or coordinate) polarities. A couple of attempts were made to change the coil centers in the model, but the problems persist (sign errors move from x to y, for example). Since it is very time consuming to sort this out after-the-fact, with incomplete or confused information, we have discontinued trying to achieve perfect agreement. We will instead adopt a strategy to make better coordinate definitions and more careful measurements during construction of the next helical solenoid model.

Figure 4.10 illustrates the coordinate system for one model, and Table 1 lists the coil center coordinates relative to the measurement system (although reflections in X,Y are possible and may explain polarity discrepancies). Fig. 4.11 shows the model geometry and predicted flux density on the coils. Transfer functions are shown in Figures 4.12 to 4.14 for the individual field components, which should be compared directly to data plotted in Figures 4.5, 4.6, 4.8, and 4.9.

Table 2. Coil centers for Magnetic Model

Coil	X, inch	Y, inch	Z, mm
1	-1.21	1.141	-90
2	-0.75	0.488	-70
3	-0.38	-0.18	-50
4	-0.01	-30	

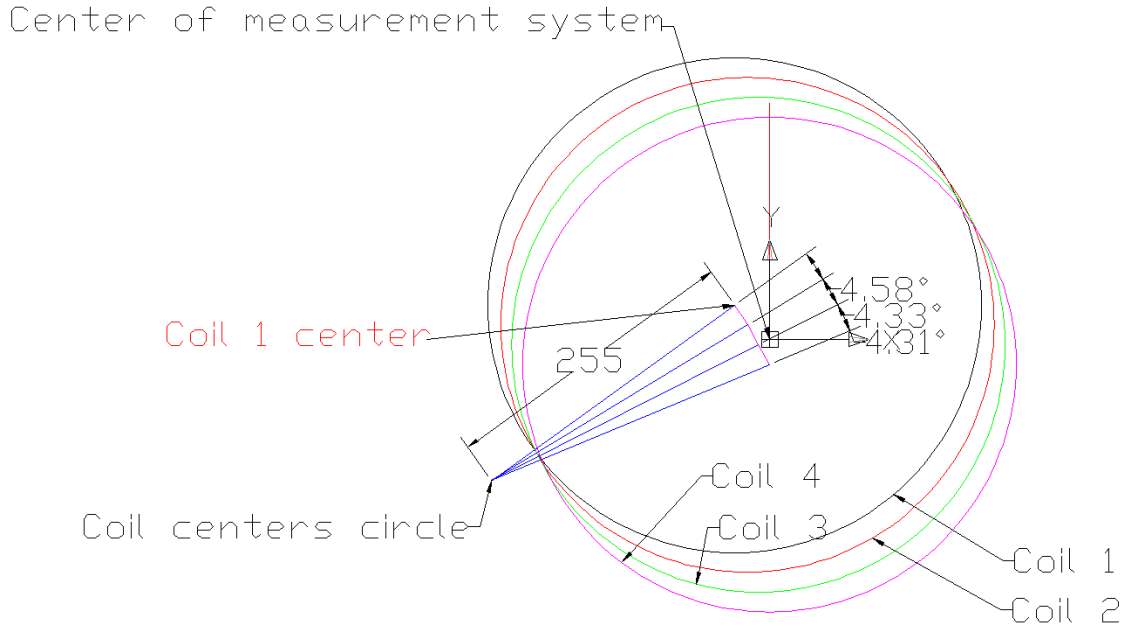


Fig. 4.10. Coil positions relative to center of measurement system

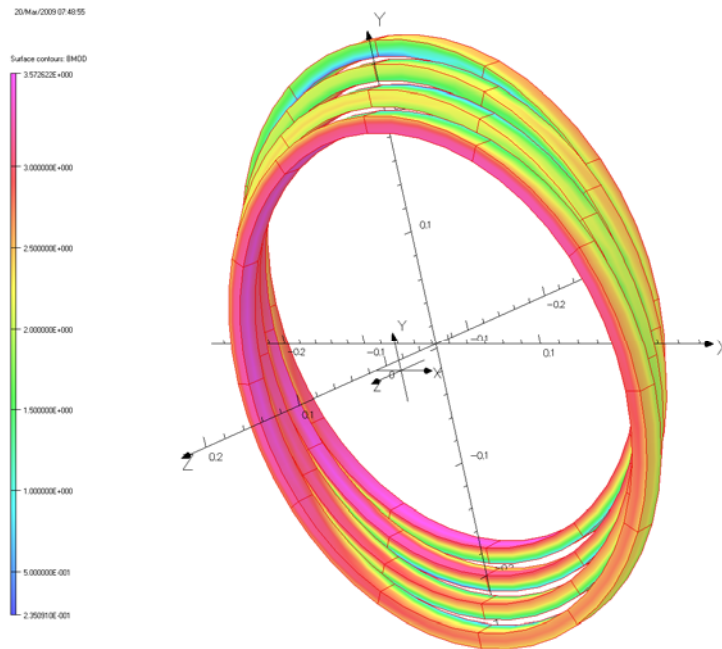


Fig. 4.11. Model geometry and flux density on coils at 10kA current.

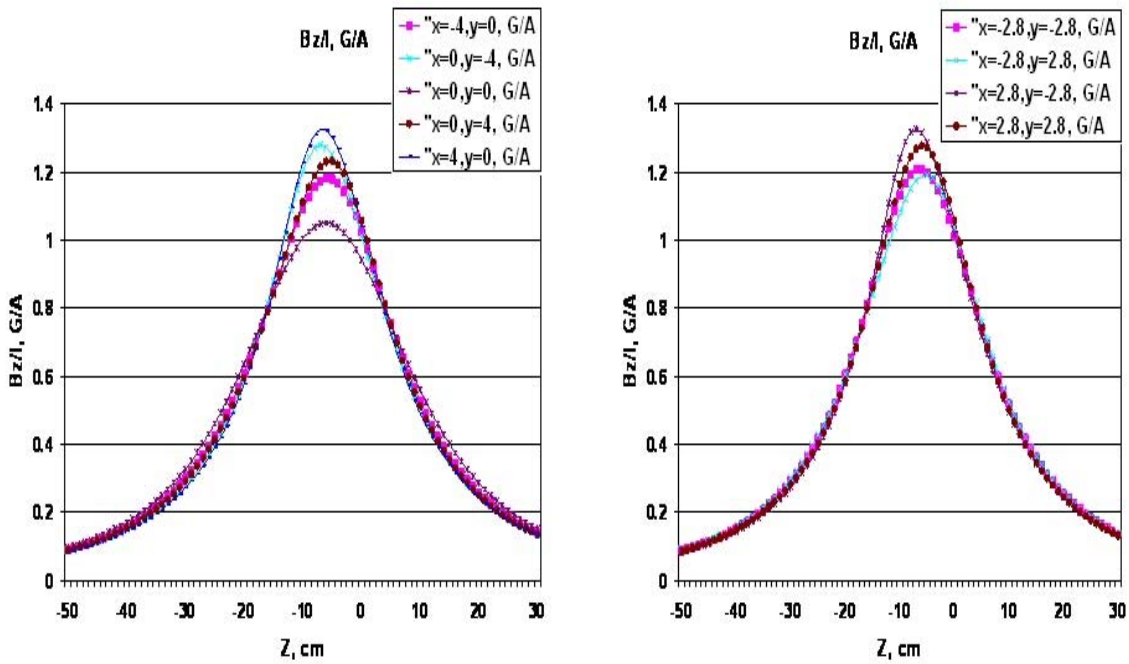


Fig. 4.12. Model predicted  $B_z/I$  field distribution along Helical Solenoid model Z-axis.

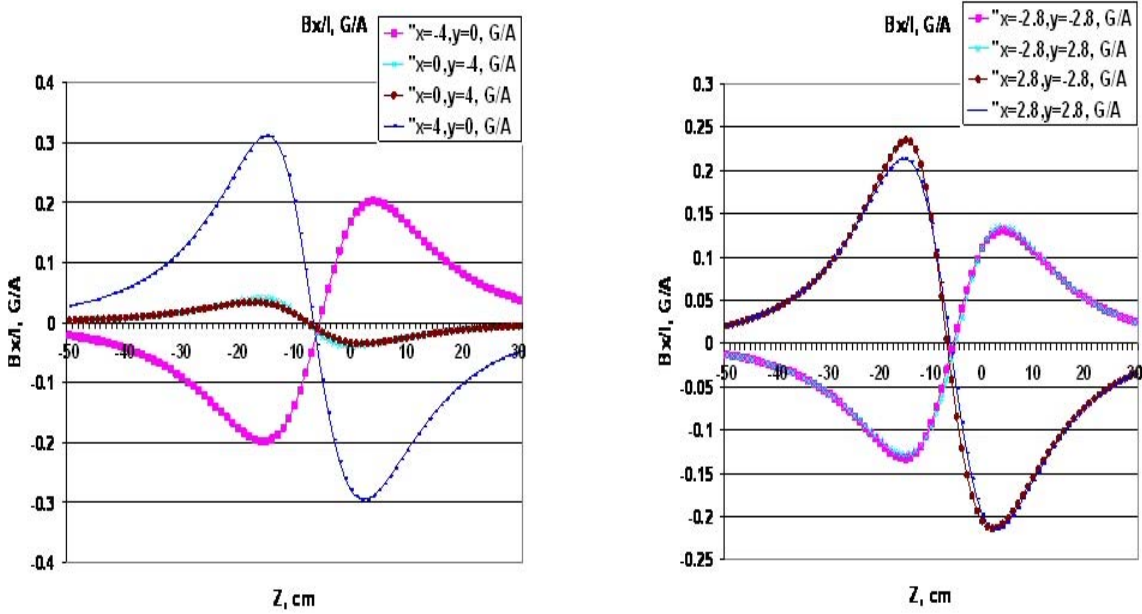


Fig. 4.13. Model predicted  $B_x/I$  field distribution along Helical Solenoid model Z-axis.

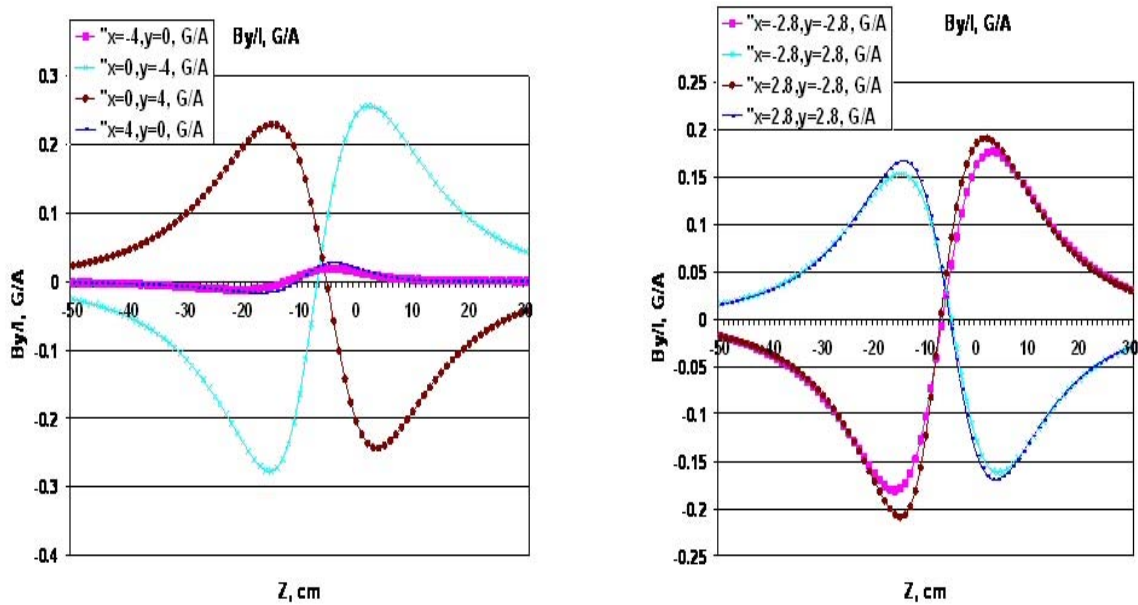


Fig. 4.14. Model predicted  $B_y/I$  field distribution along Helical Solenoid model Z-axis.

## 5. Quench Studies

### a. Expected Performance

Figure 5.1 shows the quench prediction for the as-built helical solenoid, with a total of 37 turns of 30 strand SSC inner cable in the 4 coils defining the load line. The short-sample performance of the strand was measured at 4.2 K in the TD Short Sample Test Facility. This measured performance is somewhat better than that specified in Table 1, which is a target short sample performance specification for that strand. The intersection of these curves predicts a maximum quench current of just over 16 kA. The nominal operating current to achieve the desired dipole and axial field strengths is 9.6 kA, which produces a peak magnetic field on the coil of 3.3 T.

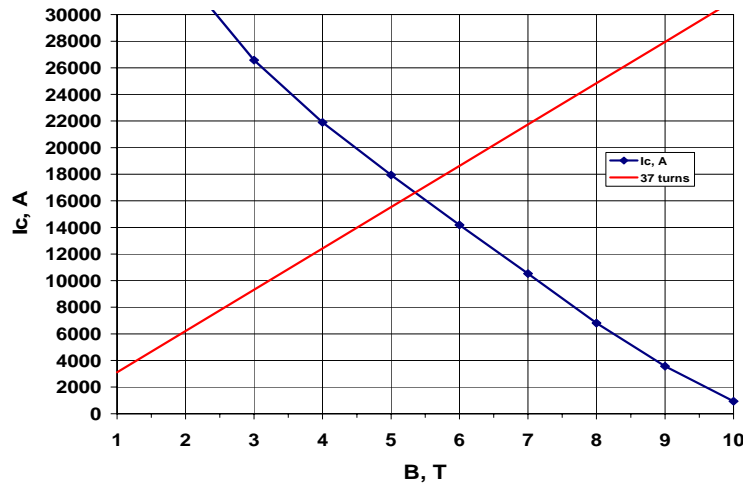


Fig. 5.1. HSM01 37-turn load line (red) and measured 4.2 K short sample curve (blue).

**b. Quench Training at 4.5 K**

Due to worries about ground current in view of the hi-pot problem, the quench training program proceeded cautiously, with close monitoring of the ground current and coil voltages after each quench event. Nevertheless it did proceed, due to the prediction that voltage development in the coils would be quite small due to the low magnet inductance. After low-current (5 kA) manual trips to check the quench protection system, magnet training was conducted at a ramp rate of 50 A/s.

Figure 5.2 shows the electrical schematic for power system connections and instrumented coil segments in the HSM01 solenoid circuit. Note that the “Coil” labels differ from the “Quadrant” Voltage Tap labels given by the T&I electrical group (and captured in quench data). For this device, the only quench characterization voltage taps were at the “quadrant” level – thus, one can determine in which coil the quench originated – by voltage taps placed between coil layers and at the superconducting leads (SCL) where they enter the mechanical structure. Half coil signals H1 and H2 were useful for purposes of quench detection and locating the quench origin.

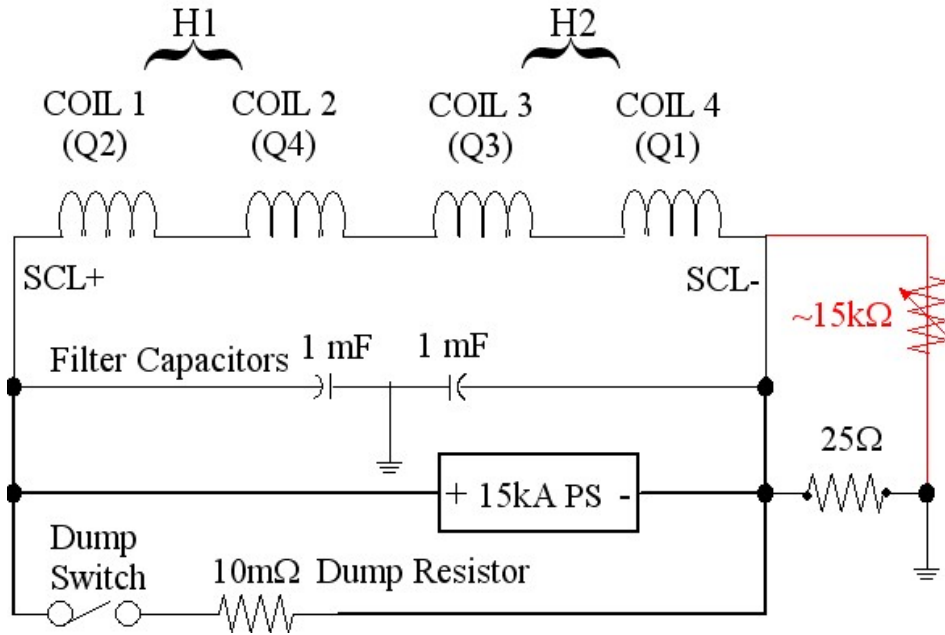


Fig. 5.2. Electrical Schematic for HSM01 Solenoid circuit at VMTF.

A summary of the quench history is shown in Figure 5.3. Numerous “trips” of the quench detection (QD) system occurred during the magnet training, in which QD circuits detected coil voltages which exceeded threshold, but data analysis indicated no actual quench had occurred. These were possibly due to problems with power supply regulation caused by the very low inductance load (however, see also section 5.f), in which the current ramp rate changed abruptly and caused an inductive voltage (or difference of two signals) that exceeded threshold. These occurrences were eliminated by changing the combination of power supplies in use (three of the six 5 kA PEI supplies in the CPS-3 system at VMTF were needed for the highest quench currents reached). The fifth quench

was unusual and puzzling in that the superconducting leads quenched. This event will be discussed in more detail later.

**c. Quench Temperature Dependence at 3.0 K**

Figure 5.3 shows that in general the magnet trained steadily upward, but with some erratic jumps down, to a rather broad quench current plateau at around  $13 \pm 1$  kA. The temperature was lowered to 3.0 K (red points) to study whether the quench current would improve due to the increase of critical current and thermal margin at lower temperature, or if the plateau was mechanically limited. As the erratic quench performance and plateau level did not improve with lowered temperature, this suggests a mechanical origin for the quenches.

**d. Ramp Rate Dependence**

A few low ramp rate tests were made at 4.5 K prior to lowering the temperature. Since no improvement in quench current was seen at lower temperature, the quench program was completed by mapping the higher ramp rate dependence (performed at the intermediate 4.0 K temperature due to cryogenic plant difficulties mentioned earlier). Strong ramp rate dependence might be expected since the metal support structure is not laminated; however, Figure 5.4 shows that there is little dependence out to 150 A/s. At higher ramp rates, 200 and 250 A/s, power supply non-regulation again caused QD system trips that did not allow us to measure the actual quench performance.

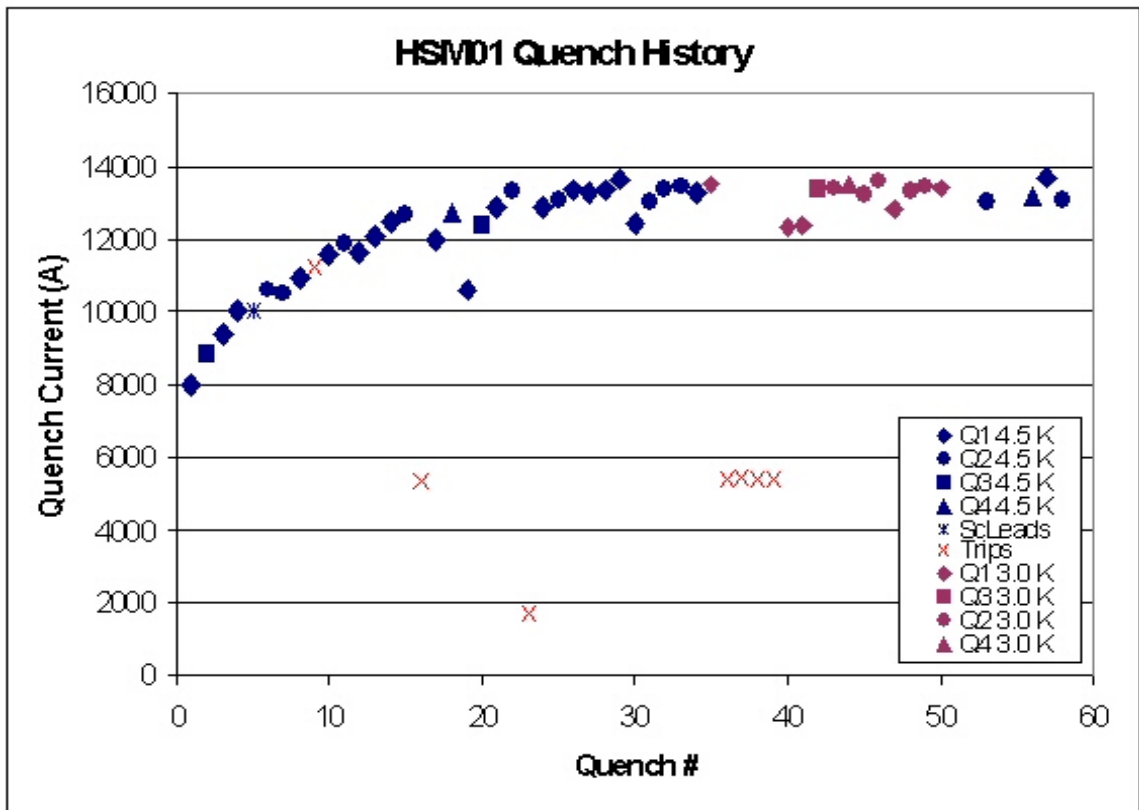


Figure 5.3. Quench history and quench locations at 4.5 K and 3 K of HSM01

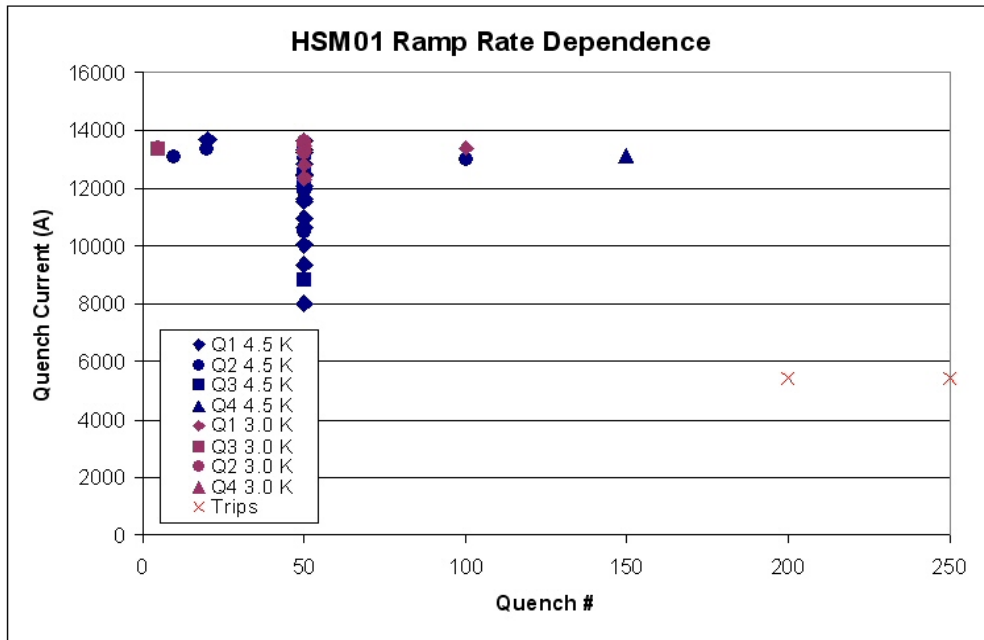


Figure 5.4. Ramp rate dependence of quench current (all quenches, including training, are shown)

**e. Quench Performance Summary**

The quench locations are coded in the symbols of Figures 5.3 and 5.4. A summary of all quench locations is shown in a frequency histogram in Figure 5.5: most quenches occurred in the coils at either end of the magnet, and most often at the end where the leads emerge. The highest quench current recorded was 13624 A in quench 29 at 4.5 K, which is roughly 85 % of the predicted maximum at that temperature. The broad quench plateau at  $13 \pm 1$  kA did not improve with lower temperature, indicating quench performance was mechanically (conductor motion) limited. No ramp rate dependence was discernable up to 150 A/s ramp rate.

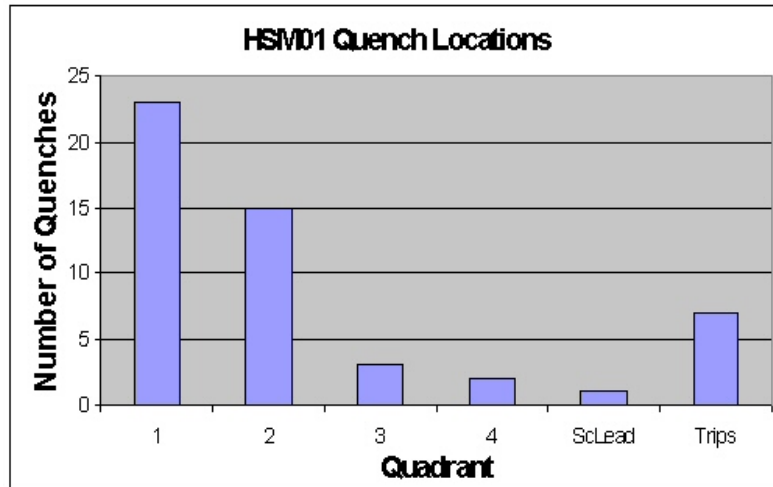


Figure 5.5. Frequency distribution of quench locations.

### f. Sc Lead Quench and Ground Current Incidents

The fifth training ramp resulted in a quench of the negative SCL. Figure 5.6 shows the voltage traces for the SCL segments, which show a sharp oscillation in both leads at 6 ms followed by voltage growth and detection of the negative lead quench in the segment between the coil and the splice to the top plate leads. No other SCL quenches occurred. However, there were numerous events in the quench program which had obvious, anomalous and steady ground current of about 57 mA prior to the quench, starting with quench 27. The ground current had been watched carefully at the beginning of the test, and not observed; the ground current detection threshold was set at 100 mA, and did not trigger any slow ramp downs. As a result, these but they went un-noticed until quench 35 (first 3.0 K quench). Figure 5.7 shows the history of ground current versus time on 12/1 and 12/2. Once it turned on, the ground current seems to have grown proportionally to the magnet current; the behavior from ramp to ramp was somewhat irregular (see Figure 5.8). It is interesting that ramps which had PS regulation-induced trips at 5 kA also had large ground current; otherwise ground current did not develop until higher magnet currents were reached!

What seems a likely scenario (based upon the post-test inspection of the leads area, described in <http://tiweb.fnal.gov/website/controller/468>) is that large Lorentz forces caused the inadequate (glass tape) SCL restraints to break on the fifth training ramp, which would result in rapid lead motion and can explain the oscillatory voltage signals and quench. On subsequent ramps the SC Leads would then move under these forces, until the negative SCL contacted the support rod bolt, and could erode layers of insulation (which would be subjected to large voltages to ground from the dump firing at 13 kA each quench).

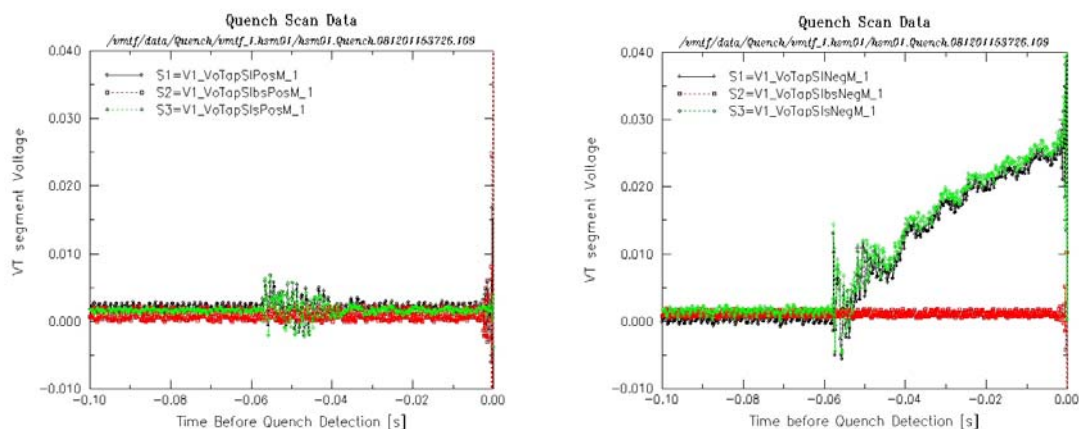


Figure 5.6. Training ramp 5 superconducting lead signals (S1 = entire lead, S1s=splice, S1bs=before splice), for positive (left) and quenching negative (right) leads.

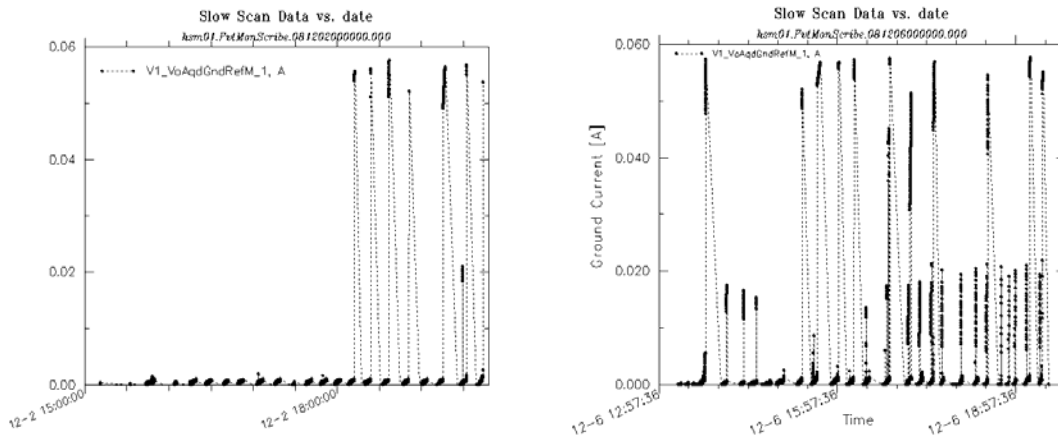


Figure 5.7. Ground current history on 12/2 (left) and 12/6 (right).

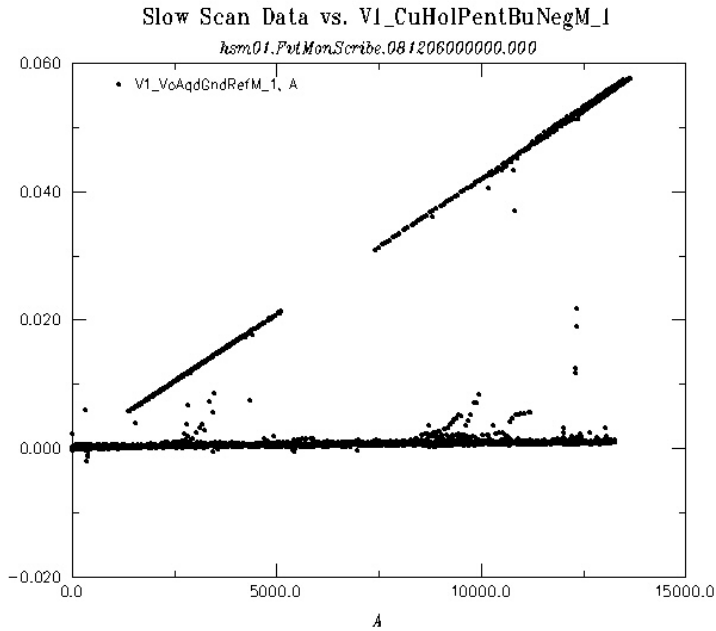


Figure 5.8. Ground current versus magnet current on 12/6 (3.0 K testing).

### 6. Heater Protection Study

Time to study heater effectiveness was limited because of the ground fault and cryogenic system problems, and was undertaken after completing the higher priority magnetic and quench performance study goals. Also, test plan options were reduced because of concerns about generating voltage in coil 4, suspected of having the ground fault. Therefore a basic test was made with coil 1 and coil 2 (full length) strip heaters connected in series to the same heater power supply (HFU), and the coil 3 and coil 4 heaters not connected. At 4.0 K with the magnet at high current, 12000 A, the heaters

were pulsed by a power supply charged to 50 V (the minimum voltage setting of this device). The first pulse was from a HFU with 4.8 mF capacitance, and a second test was then made using a second HFU set to 9.6 mF. In both cases, the heaters induced a quench in the 1<sup>st</sup> half coil, in quadrant 4 (coil 2). The time from heater firing to quench detection was 150.6 ms at 4.8 mF, and 119.2 ms at 9.6 mF.

## 7. RRR

Following the cold test, on 12/8 the VMTF dewar temperature was warmed to just above the NbTi transition temperature. The magnet was at  $10.8 \pm 0.2$  K when coil voltage measurements were made at 13:30 using the Fixed Voltage Tap (FVT) data loggers, with isolation amplifier gains set for RRR mode (attenuations of 0.01 and amplification of 100, yielding actual gains of 1.0). The individual quadrant, half, and whole coil voltages were recorded using  $\pm 10$  A current through the magnet. After warm up to room temperature (300 K at 08:43 on 12/12), these segment voltages were captured with  $\pm 5$  A through the magnet. The readout of quadrant 1 (coil 4) failed due to a poor connection at the amplifier output, so there is no result for that coil. Furthermore, the cold quadrant voltage signals are quite small and the RRR measurements are limited by the logger resolution; half and whole coil results are better (and there is not much reason to suspect coil to coil variation, since these are wound from one continuous spool of cable). The resulting RRR ratios are plotted in Figure 7.1. From the half and whole coil data, the RRR value is about 137.5.

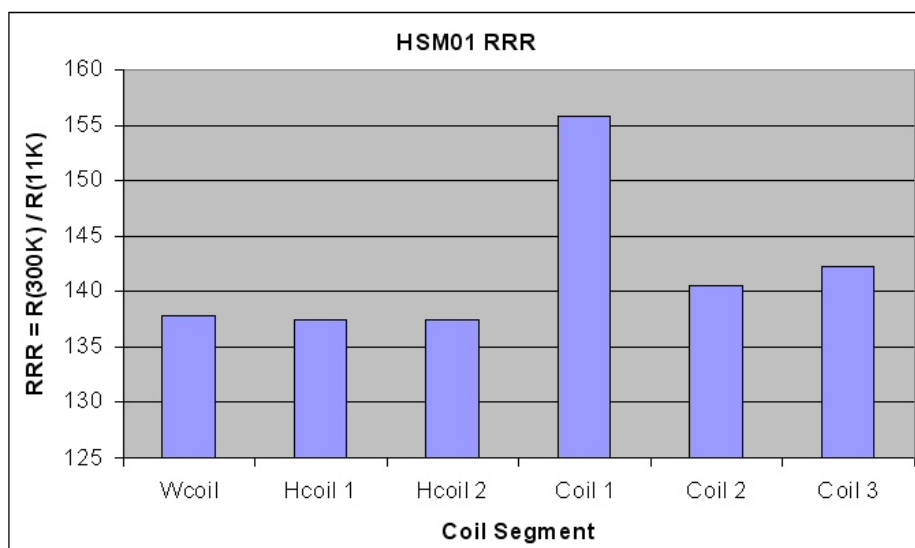


Figure 7.1. RRR values for HSM01 coil segments.

## 8. Strain Gauge Measurements

During the cool-down and magnet excitation, stress-strain is induced and the structure deforms. Strain gauges were used to monitor the strain changes on the inner and outer links and Fig.8.1 shows the locations of the gauges. T, A, L represent the strain gauges glued in transverse radial direction, azimuthal direction, and longitudinal direction respectively, and C represents compensation gauge. Strain gauge labeled with A10, which was glued on the top flange in azimuthal direction, was eliminated due to the readout being “open”.

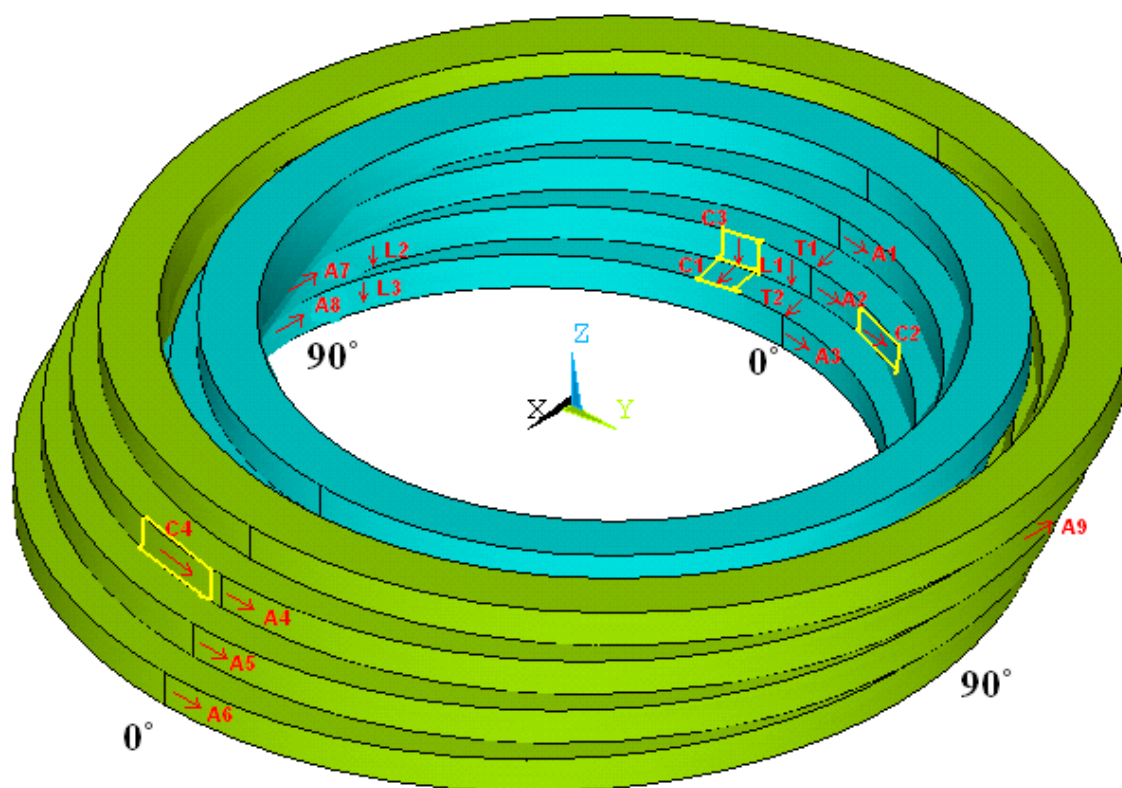


Fig. 8.1 Locations of Strain Gauges (Coil 1 is on bottom, Coil 4 is at top)

Before the magnet cool down, checkout and room temperature readout tests with 1mA excitation current were done and all strain gauges worked well.

Table 8.1 gives the readings at both warm and cold temperature. The reading on C4 is too high for a compensation gauge, and it seems like C4 was contracted together with the structure, in other words bonded with the structure, so the reading on C2 was used to replace C4 for the outer links compensation gauge. The readings on A1 and A4 are very close to the reading on the compensation gauge C2, and the readings on L1 and L3 are close to the reading on the compensation gauge C3. A possible reason is that these four gauges lost contact with the structure during cool-down and contracted only because of the sensitivity to the temperature. The transformation equation from resistance to strain is

$$\frac{\Delta R}{R_{T0}^m} = \frac{\Delta R^m}{R_{T0}^m} - \frac{\Delta R^c}{R_{T0}^c} = G \cdot \varepsilon$$

where  $\Delta R^m = R_{T1}^m - R_{T0}^m$ , is the reading change from room temperature to cold temperature of measuring strain gauge,  $\Delta R^c = R_{T1}^c - R_{T0}^c$  is the reading change from room temperature to cold temperature of compensation strain gauge, G is the gauge factor and  $\varepsilon$  is the strain. The compensated strains calculated from data are shown in Fig. 8.2 along with expectations from 3D FEM simulation.

Table 8.1 Strain Gauge Readings V at Warm and Cold Temperature with 1mA

	Warm	Cold	Difference		Warm	Cold	Difference
T1	0.350086	0.3480811	0.57%	A8	0.3494802	0.3469456	0.73%
T2	0.3501511	0.3481125	0.58%	A9	0.3497951	0.3476472	0.61%
A1	0.349982	0.3496325	0.10%	L1	0.3499246	0.3490505	0.25%
A2	0.3502628	0.3481518	0.60%	L2	0.3500575	0.3475663	0.71%
A3	0.3496045	0.3476669	0.55%	L3	0.3499261	0.3490721	0.24%
A4	0.349873	0.3494802	0.11%	C1	0.3500215	0.3493038	0.21%
A5	0.3497433	0.347681	0.59%	C2	0.3501399	0.3496868	0.13%
A6	0.3500682	0.3483299	0.50%	C3	0.3501249	0.3494969	0.18%
A7	0.3496792	0.3472634	0.69%	C4	0.3494997	0.3475231	0.57%

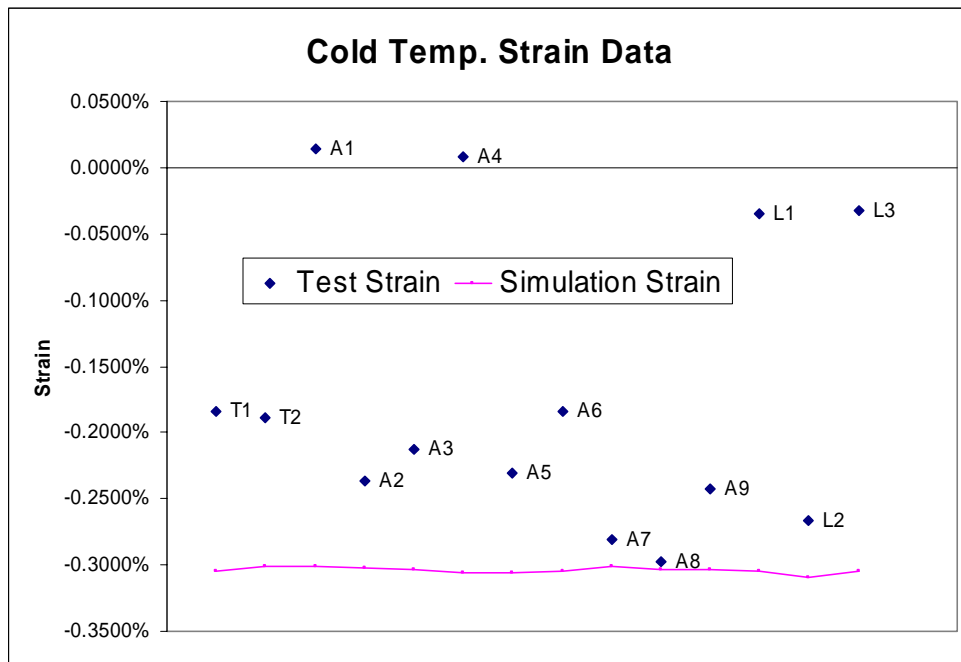
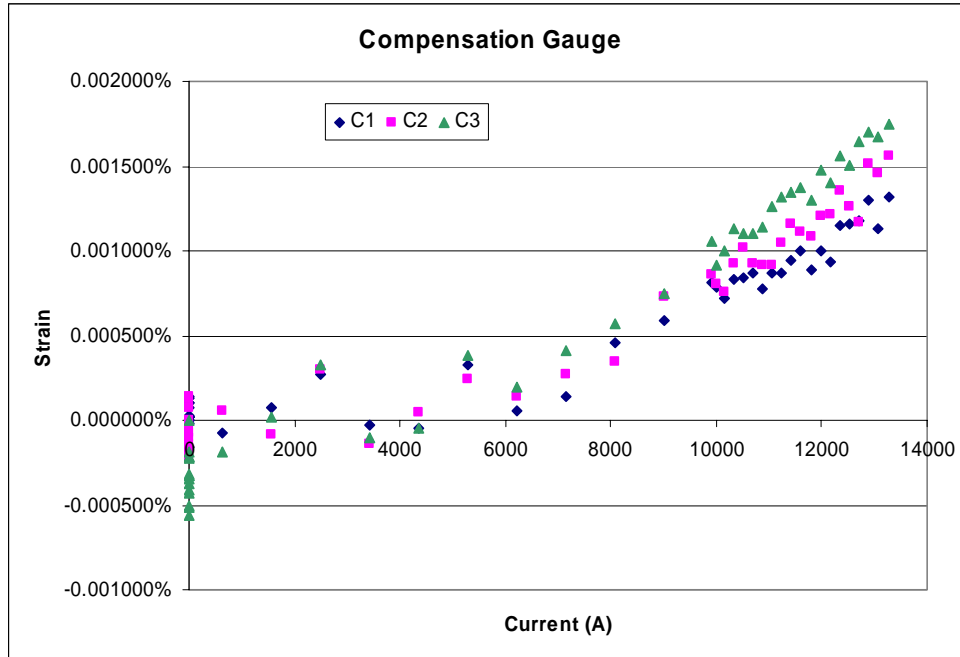
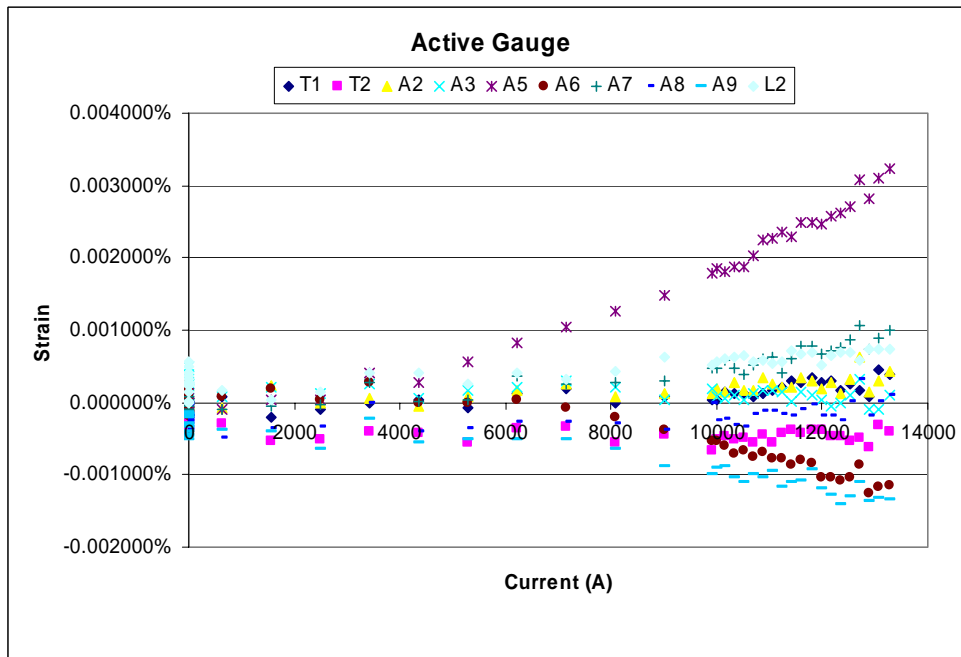


Fig. 8.2 Strain Data at Cold Temperature

During the magnet excitation, Lorentz forces are generated simultaneously with the magnetic field. From the readings on compensation gauges shown in Fig. 8.3(a), as the magnetic field increases, the magnetic field effect on the strain gauges increases in a very small range. From Fig. 8.3(b), the readings on active gauges changed a little with maximum around 0.003%, while the simulation gives about 0.007%. Compared to the 0.2~0.3 % strain from cool down, the Lorentz force strains are relatively small and very consistent with prediction.



a. Compensation Gauges

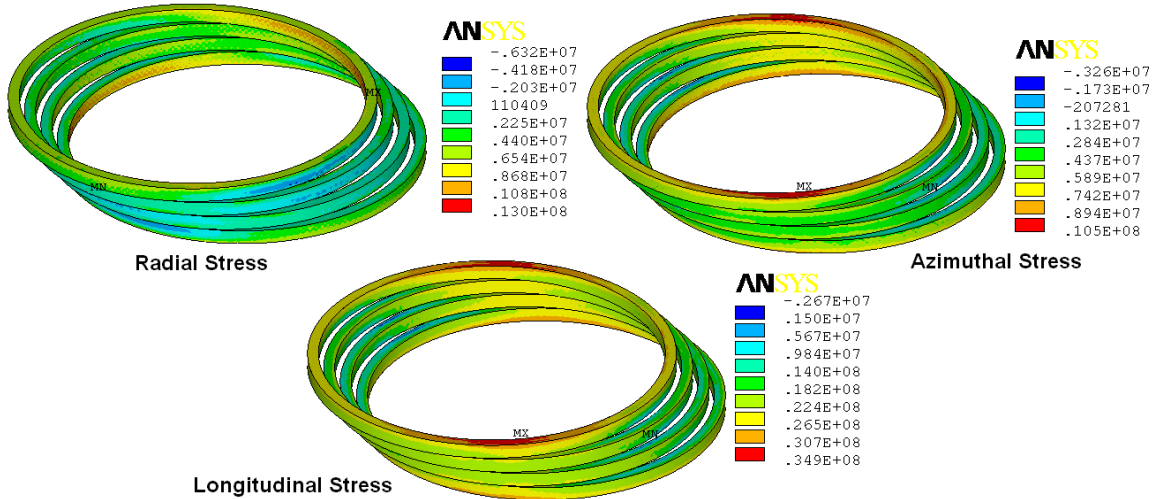


b. Active Gauges

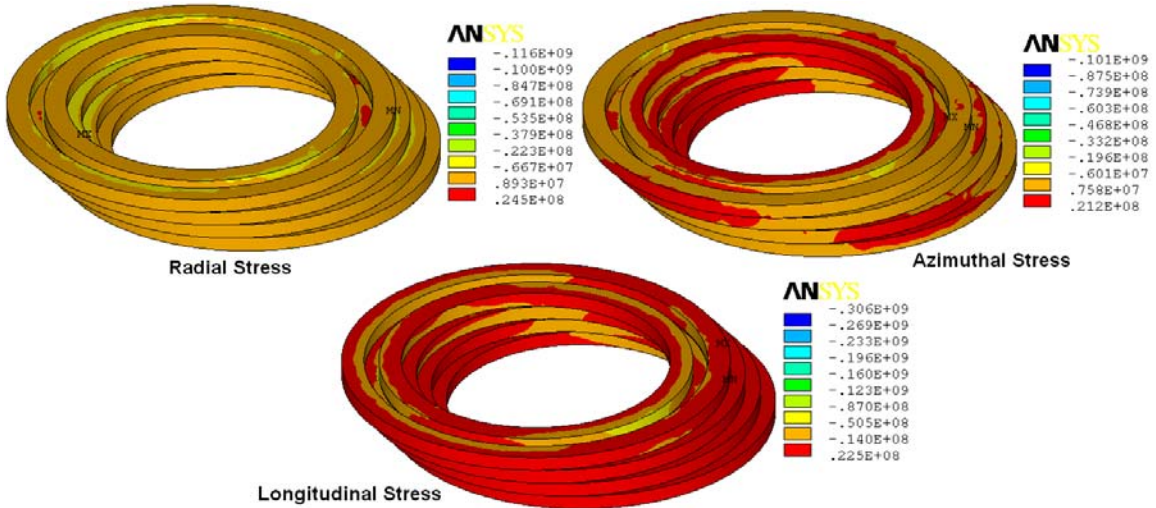
Fig.8.3. Compensation(a) and Active (b) strain gauge readings during excitation

Figures 8.4 shows the modeled stress distribution on the coils and links. For the coils, the maximum stresses in three directions (radial, azimuthal and longitudinal) are 13.0 MPa, 10.5 MPa, and 34.9 MPa respectively. For the links, the maximum stresses in three directions are 116 MPa, 101 MPa, and 306 MPa respectively. These predictions are well within the allowable 50 MPa stress for NbTi cable, and 550 MPa stress for stainless steel 304. In conclusion, we can say that the radial thickness of the inner and outer links

were designed far beyond the safety requirement for this magnet, and even for the next model with higher magnetic field obtained by using different superconductors such as Nb<sub>3</sub>Sn, the thickness of the links is still sufficient.



a. Four Coils



b. Inner and Outer Links

Fig. 8.4. Stress Distributions in Coils (a) and Links (b)

## 9. Post-Test Inspections and Autopsy Report

The model was cut following the number sequence (1-4) shown in Fig. 1, to find out if there is any mechanical limit around the coil, which may help to better understand the quench performance, etc. The purpose of cutting lines # 2 and 3 is to show the cross sections, close to the transition area, while the purpose of cutting line # 4 is to show the cross section of the lead end. Totally five pieces of cutting parts (A-E) were obtained.

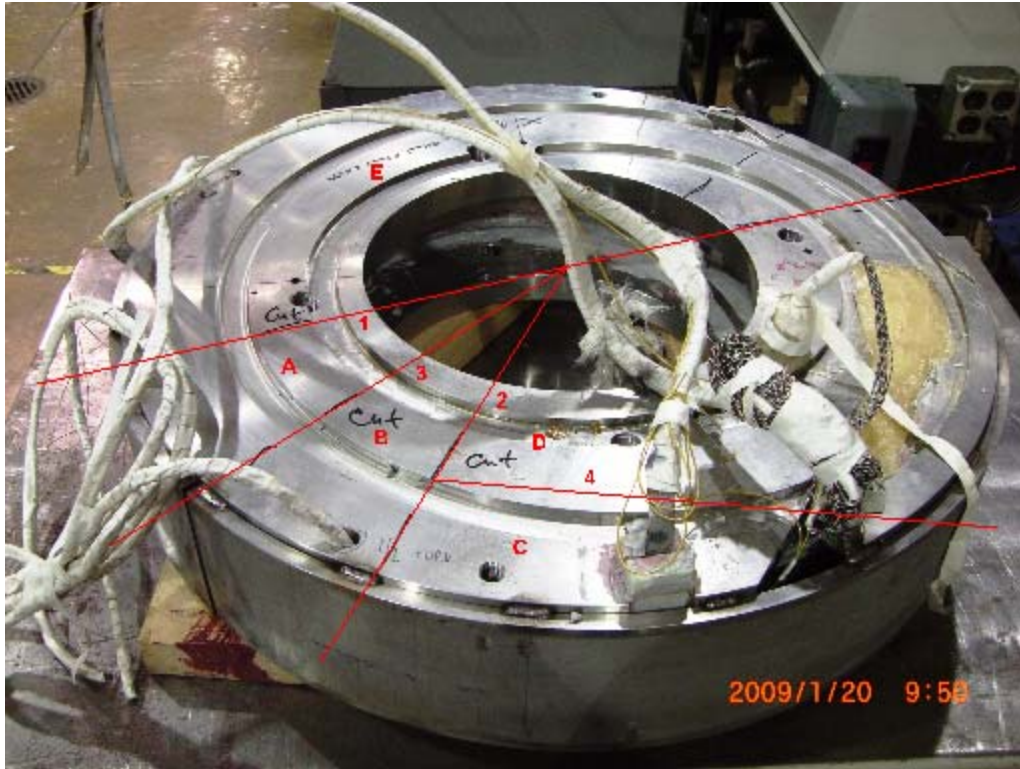


Fig. 1 Autopsy Cutting Lines (1-4) and Parts (A-E)

In the following, all the observations from the cutting photographs and measurements are listed, and then possible reasons are speculated for these observations. Fig. 2 shows both cutting surfaces of Part E, Fig.3 shows the right cutting surface of Part B, Fig.4 shows both cutting surfaces of Part B, and Fig.5 shows one cutting surface of Part A.

- From Fig. 2 left and Fig. 3, most of the voids are at upper and lower corners of the coils, between G-10 rings, as if epoxy did not penetrate.
- From Fig. 2 left, Coil#2 has 10 turns of cable, while the others have only 9 turns. The coils with 9 turns all have tilted cables, while Coil#2 with 10 turns did not obviously tilt. The keystoneed cable was wound with the thick edge on the outer diameter, which may lead to the observed tilt for those coils with one fewer turn, while the 10 turn coil is constrained by lack of space to be more flat.
- From Fig. 2 right, thicker epoxy was found between each coil and outer G-10 spacer. Thicker epoxy may crack and break down in the cold temperature more easily. The stainless steel ring grooves may have been fabricated somewhat elliptical, so that a wider gap in some regions was filled with a thicker epoxy layer.
- From Fig. 3 right, the upper left corner of the cable in Coil#2 deformed a lot and into a void region, which cannot be seen from Fig.3 left; so, the deformation must have occurred during the final machining.

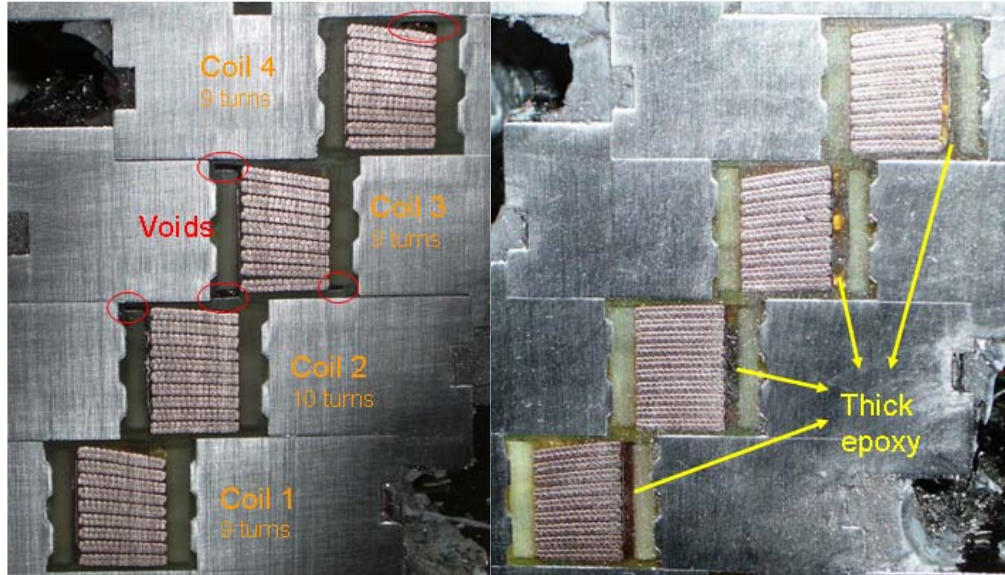


Fig. 2 Both Cutting Surfaces of Part E  
Left: The Left Cutting Surface; Right: The Right Cutting Surface

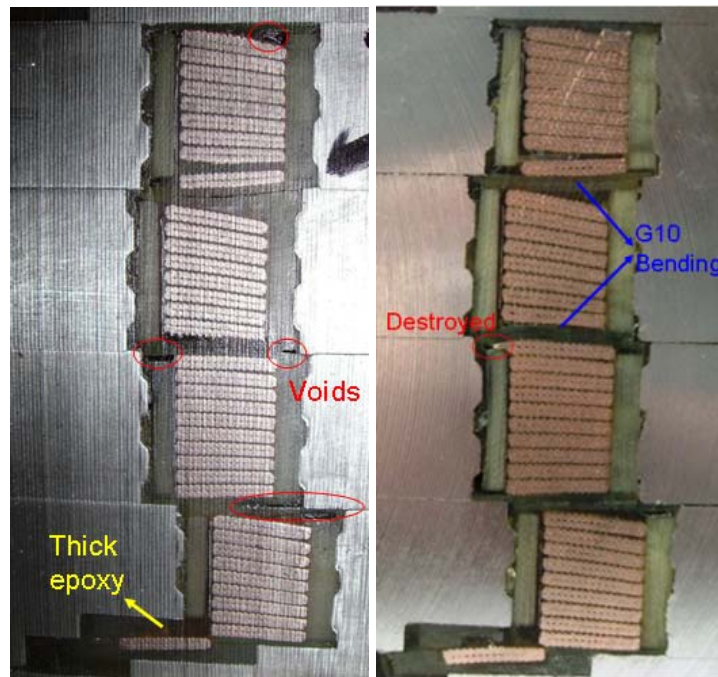


Fig.3 The Right Cutting Surface of Part B  
Left: Before Machined; Right: After Machined

- From Fig. 3 right, the G10 rings in the top and bottom of Coil#3 are bent a lot. Since there is one more turn in Coil#2, and surprisingly there are only 8 turns left in Coil#3 (details in the next bullet), Coil#2 has occupied some space from the adjacent Coil#3. Before solenoid potting, G-10 rings were compressed vertically during the winding, bending the G-10 rings.

- From Fig. 4 left, Coil#1 (including lead end cable) and Coil#2 have 10-turn cable, Coil#3 has only 8 turns and Coil#4 has 9 turns, while on the right side, Coil#2 has 10-turn cable, and the others have 9 turns. Since both surfaces belong to Part B and different small pieces of G-10 spacers were used in this special transition area, the possible reason is that these G-10 spacers were placed improperly, causing the cable misallocation in Coil#1, 2 and 3 in the transition area, which can be confirmed from the resistance measurement results (next bullet).

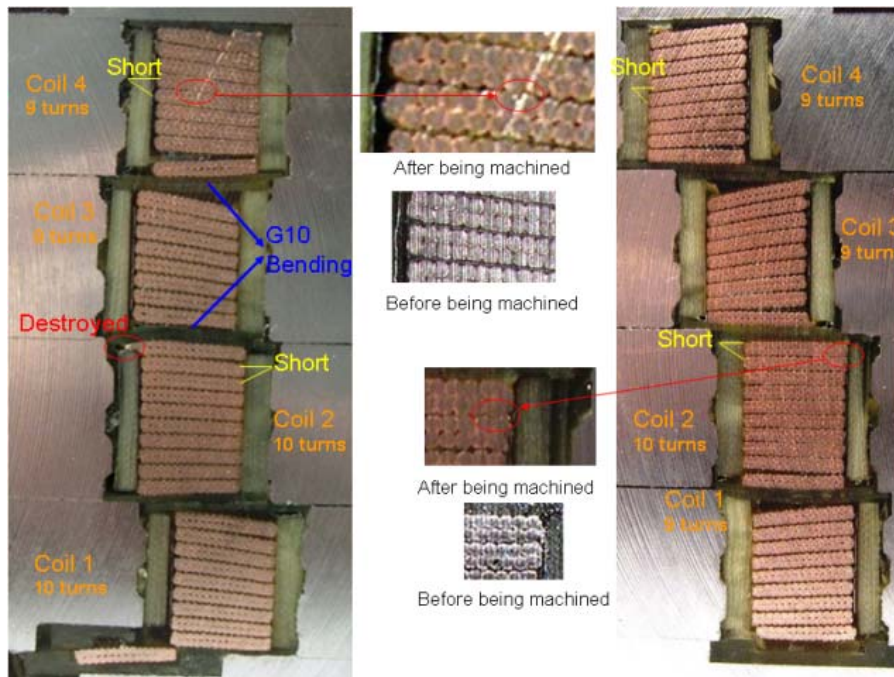


Fig.4 Both Cutting Surfaces of Part B  
 Left: The Right Cutting Surface; Right: The Left Cutting Surface

After the model was cut and machined, electrical tests were made on Parts A, B and C (See Fig. 1). Using a good Ohm meter, measurements of resistance were made for every cable in each of these sections, to adjacent cables and to ground.

- The cables were found to be insulated from each other except two pairs of adjacent cables in Part B shown in Fig. 4. In Coil#4, both sides' measurement results show short between the fourth cable and the fifth cable (counted from the top). Strangely, in Coil#2, both sides' measurement results show different short locations, one side short between the second cable and the third cable, and the other side short between the first cable and the second cable. Form Fig.4 left, it can be only explained that the first cable in Coil#2 should belong to Coil#3 which currently has only 8 turns, and then the first cable in Coil#1 should belong to Coil#2, making 10 turns for Coil#2 and 9 turns for Coil#1, which is consistence with the other cutting parts. After comparing the pictures taken before and after final machining, it is believed that the cables were deformed during the machining, causing the turn to turn short problems.
- The cables were found to be insulated from ground, with one exception: As shown in Fig.5 the bottom cable (first turn) of Coil#2 in Part A showed a reading

of  $\sim 35 \text{ M}\Omega$  to ground, (measurements with both polarities were consistent). Another measurement was taken with the same result after this surface was carefully polished using fine sand paper. At 250 V, this would yield  $\sim 7 \text{ }\mu\text{A}$  leakage current, about the right order of magnitude to be consistent with hipot results during the warm and cold test program.

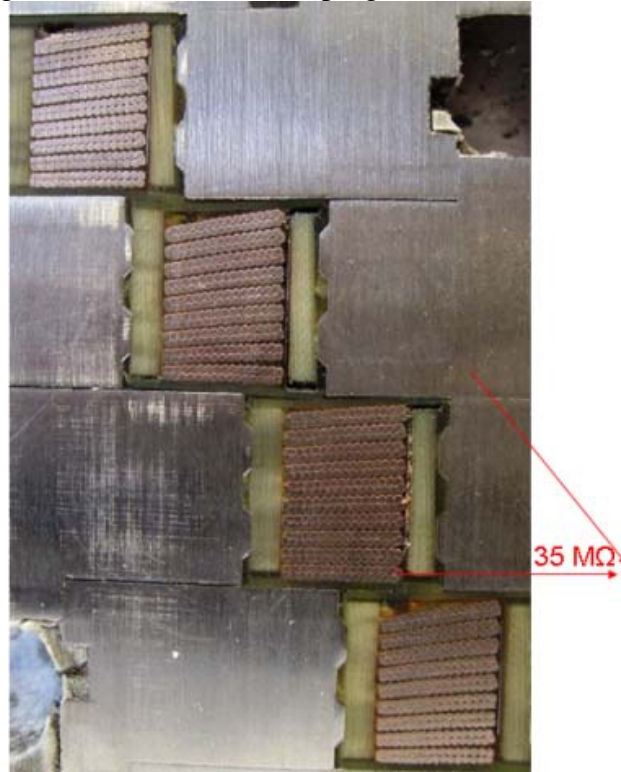


Fig. 5  $\sim 35 \text{ M}\Omega$  Found in Part A, between the First Turn of Coil#2 and the Ground

The following gives the design corrections for the HSM02:

1. The existing cable will be rolled through the cabling machine to remove key stoning at least over a half of conductor width. This will reduce the cable tilt. Also this reduces the cable thickness, which will provide enough space for 10 turns in each layer.
2. The stainless steel (SS) rings will be 22 mm thick (vs. 20 mm in original design), which will allow to increase the thickness of G-10 spacers covering the coils. Also these G-10 spacers will be much wider (+  $\sim 1/4$ " each side), which creates better insulation in transition areas.
3. Additional slots will be done in G-10 layers of inner and outer rings in the cable transition area. This shall allow us to supply Cab-O-Sil filled epoxy in these areas to prevent epoxy from cracking (there are always big voids in transition areas, which is impossible to fill with fiberglass tape).
4. Strip heaters will be placed between inner SS rings and coil in each coil layer. This creates better thermal contact between heaters and cable, and allows minimizing the gap between coil and outer SS rings (in the HSM01 heaters were

- located between outer SS rings and coil, which required additional gap between coil and outer SS rings for the heater installation). The voltage taps and strip heaters leads will be removed inside the solenoid through special slots in the inner SS rings, which prevents their damage during the outer shell installation.
5. The outer SS rings will be furnished with a copper cooling tube installed in the special slots on the outer SS rings OD. This feature will allow us to check the efficiency of the solenoid indirect cooling system.

## 10. Conclusions

The superconducting helical solenoid magnet, HSM01, was the first NbTi model built in a series of planned R&D magnets. The goals were to develop expertise and explore issues in fabrication technology, then to evaluate its mechanical, quench, and magnetic performance characteristics, and to validate structural and magnetic model predictions. This four-coil model was constrained to have the largest aperture that could fit into the vertical magnet test facility. HSM01 was fabricated and tested in 2008, and was then cut apart to carefully examine specific inner structural and electrical details to shed light on the observed performance.

This fabrication, test, and autopsy experience was rich with information and recommendations for improving the design and fabrication/test process. Unfortunately, an electrical ground fault problem limited the test program and some test elements (heater studies) were curtailed. A second NbTi model magnet design is in progress and it will incorporate the lessons learned from HSM01.

In general, HSM01 performed adequately well. Quench performance did not reach the predicted 16000 A short sample current and was limited by coil mechanical support; nevertheless the magnet trained to a current consistently above 12000 A, well above the nominal operating point of 9600 A. Stresses in the mechanical structure were measured (although not all strain gauge readings are reliable) and they agree with the finite element model predictions, which indicate that stresses in the structure are not a problem – even up to the expected maximum quench current. Magnetic field strength profiles are consistent with model predictions; however, reconciling coordinate systems and field polarities between the model and measurements turned out to be a significant challenge.

## 11. References

- [1] V. Kashikhin, et al., “Magnet System for Helical Muon Cooling Channels,” Fermilab-Conf-07-748-TD, June 2007 (Submitted to PAC ’07)
- [2] V.V. Kashikhin, et al., “Design studies of Magnet Systems for Muon Helical Cooling Channels,” Fermilab-Conf-08-286-TD, June 25, 2008 (Submitted to EPAC ’08)
- [3] V.S. Kashikhin, et al., “Four-Coil Superconducting Helical Solenoid Model for Muon Beam Cooling,” Fermilab-Conf-08-179-TD, June 25, 2008 (Submitted to EPAC ’08)